Mikada, H., Moore, G.F., Taira, A., Becker, K., Moore, J.C., and Klaus, A. (Eds.)
Proceedings of the Ocean Drilling Program, Scientific Results Volume 190/196

11. An Empirical Relationship between Velocity and Porosity for Underthrust Sediments in the Nankai Trough Accretionary Prism[1]

Nicole W. Hoffman[2] and Harold J. Tobin[2]

F1. Location of ODP Sites 1173, 1174, and 808, p. 12.

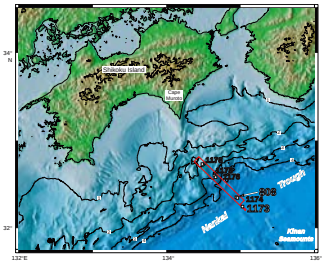

ABSTRACT

An empirical relationship between compressional wave velocity and porosity was developed for underthrust sediments in the Shikoku Basin of the Nankai accretionary prism. Shipboard core and logging measurements of velocity and porosity from Ocean Drilling Program Legs 131, 190, and 196 were used to define a new velocity-porosity transform based on an existing formulation. The new transform includes a critical porosity transition. Corrections were calculated and applied to shipboard core measurements to account for unloading from in situ conditions. The results from the velocity-porosity transform indicate the Shikoku Basin sediments follow a normal consolidation curve. A critical porosity transition is crossed at a fractional porosity of ~0.30 between the protothrust and frontal thrust zones of the accretionary prism. Although an accurate critical porosity transition was fit to these data, the critical porosity transition occurs over a range of porosity. The Shikoku Basin formulation represents a significant improvement over previous velocity-porosity formulations.

INTRODUCTION

The Nankai Trough accretionary prism of southwest Japan (Fig. F1) provides an excellent setting to study the evolution of a clastic prism.

[1]Hoffman, N.W., and Tobin, H.J., 2004. An empirical relationship between velocity and porosity for underthrust sediments in the Nankai Trough accretionary prism. *In* Mikada, H., Moore, G.F., Taira, A., Becker, K., Moore, J.C., and Klaus, A. (Eds.), *Proc. ODP, Sci. Results,* 190/196, 1–23 [Online]. Available from World Wide Web: <http://www-odp.tamu.edu/publications/190196SR/VOLUME/CHAPTERS/355.PDF>. [Cited YYYY-MM-DD]
[2]Department of Earth and Environmental Science, New Mexico Institute of Mining and Technology, 801 Leroy Place, Socorro NM 87801, USA. Correspondence author: **nhoffman@ees.nmt.edu**

Initial receipt: 5 December 2003
Acceptance: 5 August 2004
Web publication: 26 October 2004
Ms 196SR-355

Research during Ocean Drilling Program (ODP) Legs 131, 190, and 196 focused on the physical properties of the sediments in the Shikoku Basin (e.g., porosity, pore pressure, and velocity) in order to characterize both the initial state of the sediments and the alteration that occurs during initial accretion, underthrusting, and décollement formation (e.g., Moore et al., 2001).

The location of the décollement in an accretionary prism is controlled by the existence of high pore pressures in the underthrust sediments (e.g., Davis et al., 1983; Moore, 1989). Because the porosity and pore pressure in the underthrust sediments were only measured at discrete drilling locations, little is known about variations in these properties in the underthrust sediments. A conversion between marine seismic reflection velocity data and porosity would provide information on porosity variations throughout the underthrust section.

Numerous studies have been conducted to determine velocity-porosity transforms for a variety of sediment and rock types (e.g., Wyllie et al., 1958; Raymer et al., 1980). In this paper, we present a velocity-porosity transform for the Shikoku Basin underthrust sediments based on the global empirical relationship derived by Erickson and Jarrard (1998). Their analysis of high-porosity siliciclastic sediments in the Amazon Fan is based on a critical porosity formulation and accurately predicts velocity over a large range of porosity. The formulation for the Shikoku Basin sediments represents a significant improvement over previously determined relationships for the Nankai sediments (e.g., Hyndman et al., 1993).

GEOLOGIC SETTING AND SITE DESCRIPTIONS

The Nankai Trough is the subduction boundary between the Eurasian plate and the Shikoku Basin on the Philippine Sea plate. Core- and logging-based measurements obtained during ODP Legs 131, 190, and 196 from Sites 1173, 1174, and 808 define a transect across the zones of initial sediment accretion and underthrust (Figs. **F1**, **F2**). The entire underthrust section beneath the basal décollement fault was sampled at all three sites with cores and a limited number of wireline and logging-while-drilling (LWD) logs.

Site 1173 (Fig. **F2**) is the seaward reference site, where there is little evidence for tectonic deformation in the sediments. This site was sampled in order to define the state of the sediments seaward of the deformation front. Site 1174 (Fig. **F2**) is located in the protothrust zone, where there is incipient deformation and the décollement has become well developed. However, the sediments below the décollement zone show little tectonic deformation. Site 808 (Fig. **F2**) is located on the seaward edge of the imbricate thrust zone, where the décollement is already well developed. This site was sampled in order to obtain data from both the frontal thrust and décollement zones.

The sediments at Sites 1173, 1174, and 808 are primarily composed of the upper and lower Shikoku Basin facies (Fig. **F3**) (Shipboard Scientific Party, 2001b). The upper Shikoku Basin sediments vary in composition between silty clay and clayey silt and, with increasing compaction, become silty claystone and clayey siltstone. Interbedded volcanic ash layers are common, ranging in thickness from 1–2 cm up to 25 cm, with many beds 5–15 cm thick. The lower Shikoku Basin sediments are a typical hemipelagic deposit and consist predominantly of silty clay-

F2. Major structural features based on seismic reflection data, p. 13.

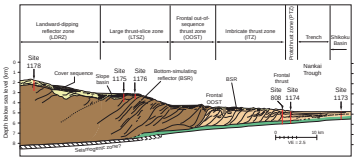

F3. Stratigraphic column, Site 1173, p. 14.

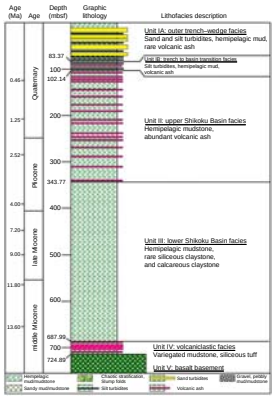

stone with scattered carbonate-cemented intervals in the middle and lower sections of the unit.

DATA AND IN SITU CORRECTIONS

A variety of core- and logging-based physical property data were collected at Sites 1173, 1174, and 808. As both velocity and porosity data are available from cores for all three sites, we used the shipboard core measurements to develop an empirical velocity-porosity relationship for the Shikoku Basin underthrust sediments. The only logging data (wireline and LWD) collected across the underthrust section were at Site 1173. The available logging data for this site were used in conjunction with the core data to determine corrections to be applied for unloading from in situ conditions.

Velocity Data

Shipboard laboratory measurements of compressional wave velocity were made on core samples from Sites 1173, 1174, and 808 (Fig. F4) (Shipboard Scientific Party, 1991, 2001c, 2001d). For unconsolidated sediments, probes were inserted into the split cores to measure transverse and longitudinal velocity. For consolidated sediments, measurements were made on samples using a Hamilton frame velocimeter contact probe system (Boyce, 1976; Hamilton, 1965). Velocity was measured in the x-, y-, and z-directions (where the z-direction is parallel to the long axis of the whole-round core section). Measurements were taken from cores collected at ~3-m intervals for Site 1173, 4-m intervals for Site 1174, and 1.5-m intervals for Site 808.

Wireline velocity data were collected at Site 1173 using the Dipole Shear Sonic Imager (DSI) tool. The DSI velocity data were reprocessed by Goldberg (this volume) using a phase-picking method to improve the quality of the logs.

Porosity Data

Porosity values for sediments from Sites 1173, 1174, and 808 (Fig. F4) (Shipboard Scientific Party, 1991, 2001c, 2001d) were obtained from shipboard laboratory measurements of moisture and density made on core samples. Wet mass, dry mass, and dry volume were measured on split core specimens. Moisture content, grain density, bulk density, and porosity were then calculated from the measured wet mass, dry mass, and dry volume values as described by Blum (1997). Measurements were taken from cores collected at ~1-m intervals for Sites 1173 and 808 and 2-m intervals for Site 1174.

Bulk density data were collected for Site 1173 (Figs. F5, F6) using the wireline Hostile Environment Litho-Density Sonde (HLDS) and the LWD Azimuthal Density Neutron (ADN) tool (Shipboard Scientific Party 2001a, 2002a). Bulk density was converted to porosity using values for mean grain density and pore water density. Measurements for both the wireline and LWD logs were collected approximately every 15 cm.

F4. Compressional velocity and porosity, p. 15.

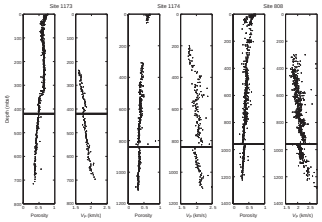

F5. Core and wireline porosity, p. 16.

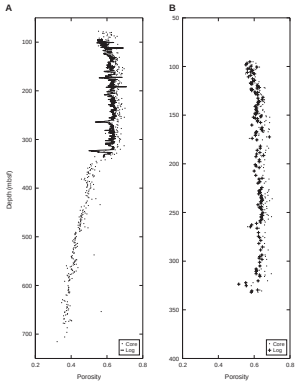

F6. Core and LWD porosity, p. 17.

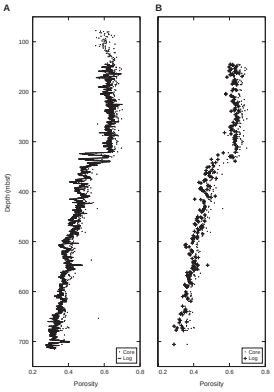

In Situ Corrections

Corrections were applied to the raw core data to account for unloading from in situ conditions. As samples are unloaded from pressure at depth, the samples undergo a decrease in grain contact stress, which causes both an increase in porosity and a decrease in seismic velocity. Corrections to velocity and porosity values were made by comparing the core data to available wireline and LWD data at corresponding depths. Because the most complete combination of core and logging data are available for Site 1173, this site was used as a standard to calculate the in situ corrections applied to core measurements from all three sites.

Porosity Correction

The Site 1173 core porosity values were compared to both wireline and LWD porosity values. As the core and logging measurements were not sampled at the same depths, a data set with matching depths was needed. Using the depths where core measurements were available, logging (wireline and LWD) data were selected for depths located ±10 cm from each core sample depth. The difference between the core and logging data sets was then calculated by subtracting the values at the matching depths. The difference between the core and logging data appears to be constant with depth when comparing the core data to both the wireline (Fig. **F5**) and LWD (Fig. **F6**) data. For the core-wireline comparison, the mean fractional porosity offset is 0.0277 ± 0.0200 (core porosity is greater than logging porosity). For the core-LWD comparison, the mean difference is 0.0307 ± 0.0249. Taking the average of these two values, the in situ correction we have chosen to apply to the core data is a constant value of 0.0289, which has an error of ±0.0224. This correction was applied to the core porosity data for Sites 1173, 1174, and 808.

Velocity Correction

The wireline DSI data from Site 1173, reprocessed by **Goldberg** (this volume), was used to determine the in situ velocity correction. The wireline velocities deviate from a general trend of increasing velocity and begin to decrease at ~345 meters below seafloor (mbsf) (Fig. **F7**), which is the boundary between the upper and lower Shikoku Basin facies. Because of this change in velocity, the in situ correction was calculated based only on the data from above ~340 mbsf.

As for the porosity data sets, core velocity and logging velocity measurements were not taken at the same depths. Using the same method described for the porosity correction, logging data were selected for depths located ±20 cm from each core depth. The difference between the core and logging data was calculated by subtracting the data sets at the matching depths.

The difference between the core and wireline velocities is expected to increase with depth (e.g., Hamilton, 1979); however, the standard deviation of the mean difference between the data sets is too large for any depth-dependent trend to be apparent. Instead, we have chosen to use the average difference between the core and wireline velocity data of 43.39 m/s (with an error of ±29.05 m/s) as a constant in situ correction. This correction was subtracted from the core velocity data for Sites 1173, 1174, and 808.

F7. Core and wireline velocity, p. 18.

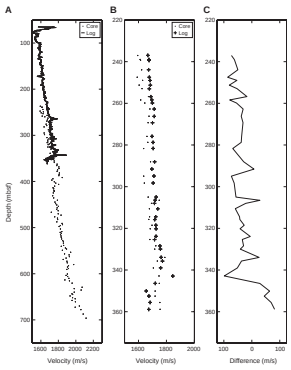

VELOCITY-POROSITY RELATIONSHIP

The Shikoku Basin and Nankai accretionary prism sediments have been well imaged using seismic reflection methods (Bangs et al., 1999; Moore et al., 1999). Seismic velocity data are important for providing information about the large-scale structure of the prism. Other physical properties of the sediments are important for understanding prism hydrology, sediment mechanical properties, and deformation styles (see Shipboard Scientific Party, 2001b). A conversion between seismic velocity and porosity would provide information about regional porosity variations in the underthrust sediments by allowing a conversion of marine seismic reflection data to porosity.

Numerous studies have been conducted in order to determine a relationship between compressional velocity (or acoustic velocity) and porosity for a variety of sediment and rock types. One of the earliest and most widely used transforms is the Wyllie time-average equation (Wyllie et al., 1958). This relationship is only reliable for consolidated sandstones over a small porosity range of 25%–30% (Raymer et al., 1980). However, corrections need to be made to apply the transform to unconsolidated sediments. An improved version of the time-average equation, developed by Raymer et al. (1980), eliminates the need for a compaction factor correction but requires the use of a separate equation for each of three porosity ranges. As neither the Wyllie time-average equation nor the formulation suggested by Raymer et al. (1980) adequately fit the Nankai sediments, Hyndman et al. (1993) used the results of Jarrard et al. (1989) and Han et al. (1986) to fit a smooth polynomial to Site 808 data. This fitted polynomial is applicable for a porosity range of ~30%–60% using a clay content of 50%.

In order to improve further on previous studies and to determine a relationship that accurately predicts over a large range of porosity, Erickson and Jarrard (1998) completed a statistical analysis of unconsolidated, high-porosity siliciclastic sediments from the Amazon Fan to develop a global velocity-porosity relationship. They identified three dominant variables affecting compressional wave velocity: porosity, shale fraction, and consolidation history. A key element of their formulation is the presence of a critical porosity, or a porosity threshold, across which the relationship between velocity and porosity fundamentally changes.

Critical Porosity

Raymer at al. (1980) recognized the concept of two separate porosity domains in which velocity exhibits different behaviors. The suspension domain for high-porosity rocks describes a medium where solid particles are suspended in the fluid. The consolidated rock domain for low-porosity rocks describes a medium with a continuous frame-supported matrix. Nur et al. (1998) define this transition from a suspension to a continuous matrix as the critical porosity. Most importantly, the critical porosity transition divides the relationship between velocity and porosity into two domains. For porosities greater than the critical porosity, velocity is not strongly dependent on porosity. For values below the critical porosity, velocity depends strongly on porosity and increases significantly with a small decrease in porosity.

It is important to note that the existence of a critical porosity transition does not indicate the transition from a zero-strength suspension to

a frame-supported regime, but rather a transition where the frame modulus increases beyond a threshold and causes a substantial velocity increase (Erickson and Jarrard, 1998).

Shale Fraction

Clay content was evaluated by Erickson and Jarrard (1998) as a possible third-order factor affecting compressional wave velocity. The physical dependence is indirect: clay content can affect porosity, which, in turn, affects velocity. Also, lithology directly affects velocity through matrix density and matrix velocity. By removing the effects of porosity and pressure to calculate residual velocities, Erickson and Jarrard (1998) determined that clay content has no direct influence in high-porosity sediments. They suggest for high-porosity sediments that the bulk modulus is dominated by the pore fluid modulus and lithology-dependent variations in the matrix bulk modulus are overwhelmed. However, clay content is assumed to be an important control on velocity for porosities of <30% through its direct effect on the aggregate and frame bulk moduli (Erickson and Jarrard, 1998).

Because quantitative clay content data were not generally available for their logging-based study, Erickson and Jarrard (1998) used an empirical "shale fraction" log that is loosely predictive of clay content. The shale fraction log (v_{sh}) can be calculated by using the gamma ray log and the nonlinear response function for Tertiary rocks (Dresser Atlas, 1982):

$$v_{sh} = 0.083 \times 2^{((3.7 \times IGR) - 1)} \quad (1)$$

where IGR = $(GR_{log} - GR_{sand})/(GR_{shale} - GR_{sand})$. The terms GR_{log}, GR_{sand}, and GR_{shale} are the gamma ray (GR) values in API units. The sand (GR_{sand}) and shale (GR_{shale}) baselines are the minimum and maximum values, respectively, in the gamma ray log.

Consolidation History

Consolidation is known to affect the compressional velocities for high-porosity sediments (Blangy et al., 1993) by not only affecting the porosity but also the shear and frame bulk moduli by increasing intergrain contacts (Erickson and Jarrard, 1998). To account for this, separate velocity-porosity relationships have been determined for what are termed "normally" and "highly" consolidated sediments. High consolidation is often seen with accretionary prism deformation, early cementation, or deep burial. Sedimentary basins are an example of a normal consolidation environment.

Empirical Velocity-Porosity Relationships

The global empirical relationships for compressional wave velocity (V_P) in terms of fractional porosity (ϕ), shale fraction (v_{sh}), and consolidation history are (Erickson and Jarrard, 1998) as follows. Normal consolidation (Fig. F8):

$$V_P = 0.739 + 0.552\phi + 0.305/[(\phi + 0.13)^2 + 0.0725]$$

$$+ 0.61(v_{sh} - 1.123)[X_1], \quad (2)$$

F8. Compressional velocity vs. porosity and shale fraction, p. 19.

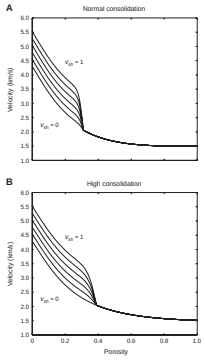

where X_1 = tanh[40(ϕ – ϕ_c)] – |tanh[40(ϕ – ϕ_c)]|; critical porosity (ϕ_c) = 0.31.

High consolidation (Fig. F8):

$$V_P = 1.11 + 0.178\phi + 0.305/[(\phi + 0.135)^2 + 0.0775] + 0.61(v_{sh} - 1)[X_2], \quad (3)$$

where X_2 = tanh[20(ϕ – ϕ_c)] – |tanh[20(ϕ – ϕ_c)]|; critical porosity (ϕ_c) = 0.39.

SHIKOKU BASIN VELOCITY-POROSITY RELATIONSHIP

In situ corrected core-based measurements of velocity and porosity were used for the underthrust sediments from Sites 1173, 1174, and 808 to determine the formulation for the velocity-porosity relationship (Fig. F4). For the core velocity values, only measurements in the z-direction were used, as they correspond to seismic interval velocities.

Shale Fraction

A shale fraction was calculated for the Site 1173 underthrust sediments (Fig. F9) based on Equation 1 using the LWD gamma ray log. The sand and shale baselines were determined from the LWD gamma ray log for Site 808, as there were no clean sands at Site 1173 from which to determine these values. The average shale fraction for Site 1173 was calculated to be 0.32.

F9. Calculated shale fraction log, Site 1173, p. 20.

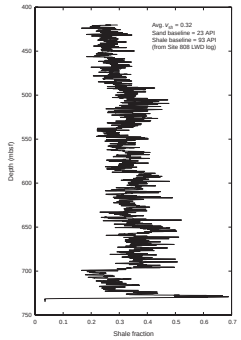

Parameter Fitting

The functional form of Equations 2 and 3 are used to determine a velocity-porosity relationship for the Shikoku Basin underthrust sediments. New parameters were determined using an implementation of the nonlinear least-squares Marquardt-Levenberg algorithm. The starting parameters for the fitting algorithm were obtained from the normal consolidation equation (Eq. 2). The parameters fit in the analysis are A, B, C, v_{sh}, and ϕ_c (Eq. 4). The form of the equation fit using the nonlinear least-squares method is

$$V_P = A + B\phi + 0.305/[(\phi + C)^2 + 0.305/(1.51 - A - B) - C^2 - 2C - 1] + 0.61(v_{sh} - 1.123)[X_m], \quad (4)$$

where X_m = tanh[40(ϕ – ϕ_c)] – |tanh[40(ϕ – ϕ_c)]|. This equation incorporates the boundary condition of V_P = 1.51 km/s at a fractional porosity of 1.

F10. Velocity vs. porosity for in situ corrected core data, p. 21.

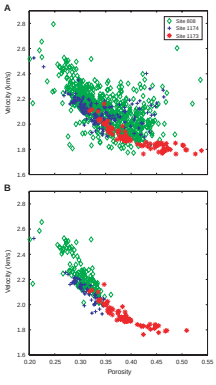

RESULTS

Velocity vs. porosity is plotted for the in situ corrected core data for all three sites (Fig. F10). These data are plotted for both above and below the décollement (Fig. F10A) and then for below the décollement

only (Fig. F10B). The plot for data above and below the décollement does not show a significant trend of increasing velocity with decreasing porosity, whereas there is a much more obvious trend for the underthrust sediments. The bounding equations from Erickson and Jarrard (1998) for normal and high consolidation are also plotted for the underthrust sediments (Fig. F11). The underthrust data lie mostly within the bounds of these equations but follow the normal consolidation trend more closely.

The fitted parameters are listed in Table T1, which includes the sensitivity of the fit to each parameter. The parameters for Equations 2 and 3 are also listed for comparison. The root mean square (RMS) of the residuals for these parameters is ±73.34 m/s. The best-fit formulation is plotted in Figure F11.

In addition to the Erickson and Jarrard (1998) formulations, the velocity-porosity relationship from Hyndman et al. (1993) for Site 808 is plotted for comparison (Fig. F11). Porosity (ϕ) is given in terms of compressional velocity (V in km/s):

$$P = -1.180 + 8.607(1/V) - 17.89(1/V)^2 + 13.94(1/V)^3. \quad (5)$$

DISCUSSION

The velocity vs. porosity plots for the sediments from Sites 1173, 1174, and 808 (Fig. F10A, F10B) clearly indicate that the sediments above and below the décollement exhibit different tectonic histories. This is illustrated by the absence of a trend in increasing velocity with decreasing porosity. This is most likely due both to a more varied lithology in the sediments above the décollement and to differing tectonic histories. In addition, the abnormal compaction trend observed in the Upper Shikoku Basin sediments may also contribute to the scatter observed in the velocity vs. porosity plots. An abnormal compaction trend is indicated by the constant velocities and high porosities present in this interval, which are most likely caused by cementation related to the processes of silica diagenesis (see Shipboard Scientific Party, 2001b, 2002b).

When only the underthrust sediments are plotted (Fig. F10B), a clear trend of increasing velocity with decreasing porosity and a critical porosity transition are apparent. This is especially true for Site 808 data and, to a lesser extent, Site 1174 data. The underthrust sediments follow the normal consolidation trend proposed by Erickson and Jarrard (1998) as is expected for underthrust sediments that have been subjected only to burial compaction stresses (Davis et al., 1983; Morgan and Karig, 1995).

The results of the parameter fitting for the underthrust sediments indicate that a critical porosity transition is crossed at ~0.30. Although a single critical porosity value can be accurately fit to this data set, it appears that the critical porosity transition occurs over a range of porosities for Site 808. The median value of this range is ~0.31, which agrees relatively well with the value obtained in the parameter fitting.

The parameter fitting provided a best-fit shale fraction value of ~1.06. One possible explanation for an unphysical shale fraction being fit is the lack of lower-porosity, higher-velocity data to constrain this parameter. The average shale fraction of 0.32 calculated from the shale fraction log (Fig. F9) suggests that a lower value would more accurately describe Site 1173 data. However, the shale fraction log for Site 1173 is

F11. Velocity-porosity for the underthrust sediments, p. 22.

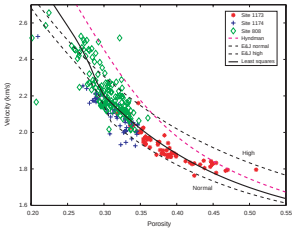

T1. Parameter fitting for best-fit formulation, p. 23.

probably not accurate due to the lack of representative sand and shale baselines. Further analysis needs to be done to accurately determine which shale fraction best describes the Shikoku Basin underthrust sediments.

It is also important to note that the value of the shale fraction significantly affects the values determined for the critical porosity in the parameter fitting. An improved fit could probably be obtained by holding the shale fraction constant (at a value representative of the sediments at Site 1173) and allowing the critical porosity to vary.

The relationship derived by Hyndman et al. (1993) does not appear to fit either the lower- or higher-porosity sediments as well as the formulations suggested by Erickson and Jarrard (1998). The Hyndman et al. (1993) formulation does follow roughly the same trend but generally overestimates the velocity, especially for porosities near the critical porosity transition. However, this formulation was derived only for Site 808 data, and different in situ corrections have been applied to the current core data set, which could account for some of the differences.

CONCLUSIONS

The underthrust sediments from Sites 1173, 1174, and 808 follow the global velocity-porosity trends proposed by Erickson and Jarrard (1998). The formulation for normal consolidation is a better fit to the data than the high-consolidation model, as is expected for tectonically undeformed underthrust sediments.

New parameters fit to the normal consolidation model using a standard nonlinear least-squares algorithm provides a single best-fit equation that can be used to convert between velocity and porosity with reasonable uncertainty. This formulation will be used to predict porosity from seismic interval velocity for the underthrust sediments. The new formulation better predicts velocity than any of the previously determined relationships.

A critical porosity threshold appears to be crossed somewhere between Sites 1174 and 808, at ~0.30. Although a single critical porosity value can be reliably fit to the data, there are a range of porosities for which velocity exhibits a stronger dependence on porosity.

ACKNOWLEDGMENTS

This research used samples and data provided by the Ocean Drilling Program (ODP). ODP is sponsored by the U.S. National Science Foundation (NSF) and participating countries under management of Joint Oceanographic Institutions (JOI), Inc. A research assistantship for N. Hoffman was provided by JOI and U.S. Science Support Program (USSSP) postcruise funding for ODP Leg 190. The authors wish to thank J.C. Moore for helpful suggestions and Lorri Peters for editorial review.

REFERENCES

Bangs, N.L., Taira, A., Kuramoto, S., Shipley, T.H., Moore, G.F., Mochizuki, K., Gulick, S.S., Zhao, Z., Nakamura, Y., Park, J.-O., Taylor, B.L., Morita, S., Ito, S., Hills, D.J., Leslie, S.C., Alex, C.M., McCutcheon, A.J., Ike, T., Yagi, H., and Toyama, G., 1999. U.S.–Japan collaborative 3-D seismic investigation of the Nankai Trough plate-boundary interface and shallowmost seismogenic zone. *Eos, Trans. Am. Geophys. Union,* 80:569.

Blangy, J.P., Strandeness, S., Moos, D., and Nur, A., 1993. Ultrasonic velocities in sands—revisited. *Geophysics,* 58:344–356.

Blum, P., 1997. Physical properties handbook: a guide to the shipboard measurement of physical properties of deep-sea cores. *ODP Tech. Note,* 26 [Online]. Available from World Wide Web: <http://www-odp.tamu.edu/publications/tnotes/tn26/INDEX.HTM>. [Cited 2003-12-05]

Boyce, R.E., 1976. Definitions and laboratory techniques of compressional sound velocity parameters and wet-water content, wet-bulk density, and porosity parameters by gravimetric and gamma-ray attenuation techniques. *In* Schlanger, S.O., Jackson, E.D., et al., *Init. Repts. DSDP,* 33: Washington (U.S. Govt. Printing Office), 931–958.

Davis, D., Suppe, J., and Dahlen, F.A., 1983. Mechanics of fold-and-thrust belts and accretionary wedges. *J. Geophys. Res.,* 88:1153–1172.

Dresser Atlas, 1982. *Well Logging and Interpretation Techniques, The Course for Home Study* (3rd ed.): USA. (Dresser Atlas Industries).

Erickson, S.N., and Jarrard, R.D., 1998. Velocity-porosity relationships for water-saturated siliciclastic sediments. *J. Geophys. Res.,* 103:30385–30406.

Hamilton, E.L., 1965. Sound speed and related properties of sediments from Experimental Mohole (Guadalupe Site). *Geophysics,* 30:257–261.

Hamilton, E.L., 1979. Sound velocity gradients in marine sediments. *J. Acoust. Soc. Am.,* 65:909–921.

Han, D., Nur, A., and Morgan, D., 1986. Effects of porosity and clay content on wave velocities in sandstones. *Geophysics,* 51:2093–2107.

Hills, D.J., Moore, G.F., Bangs, N.L., Gulick, S.S., and Leg 196 Shipboard Scientific Party, 2001. Preliminary results from integration of 2D PSDM and ODP Leg 196 LWD velocity data in the Nankai accretionary prism. *Eos, Trans. Am. Geophys. Union,* 82:F1221. (Abstract)

Hyndman, R.D., Moore, G.F., and Moran, K., 1993. Velocity, porosity, and pore-fluid loss from the Nankai subduction zone accretionary prism. *In* Hill, I.A., Taira, A., Firth, J.V., et al., *Proc. ODP, Sci. Results,* 131: College Station, TX (Ocean Drilling Program), 211–220.

Jarrard, R.D., Dadey, K.A., and Busch, W.H., 1989. Velocity and density of sediments of Eirik Ridge, Labrador Sea: control by porosity and mineralogy. *In* Srivastava, S.P., Arthur, M.A., Clement, B., et al., *Proc. ODP, Sci. Results,* 105: College Station, TX (Ocean Drilling Program), 811–835.

Moore, G.F., Taira, A., Klaus, A., and Leg 190 Scientific Party, 2001. New insights into deformation and fluid flow processes in the Nankai Trough accretionary prism: results of Ocean Drilling Program Leg 190. *Geochem. Geophys. Geosyst.,* 2:10.1029/2001GC000166.

Moore, G.F., Taira, A., Kuramoto, S., Shipley, T.H., and Bangs, N.L., 1999. Structural setting of the 1999 U.S.–Japan Nankai Trough 3-D seismic reflection survey. *Eos,* 80:F569.

Moore, J.C., 1989. Tectonics and hydrogeology of accretionary prisms: role of the décollement zone. *J. Struct. Geol.,* 11:95–106.

Morgan, J.K., and Karig, D.E., 1995. Décollement processes at the Nankai accretionary margin, Southeast Japan. *J. Geophys. Res.,* 100:15221–15231.

Nur, A., Mavko, G., Dvorkin, J., and Galmudi, D., 1998. Critical porosity: a key to relating physical properties to porosity in rocks. *Leading Edge,* 17:357–362.

Raymer, L.L., Hunt, E.R., and Gardner, J.S., 1980. An improved sonic transit time-to-porosity transform. *Trans. SPWLA 21st Annu. Log. Symp.,* P1–P13.

Shipboard Scientific Party, 1991. Site 808. *In* Taira, A., Hill, I., Firth, J.V., et al., *Proc. ODP, Init. Repts.,* 131: College Station, TX (Ocean Drilling Program), 71–269.

Shipboard Scientific Party, 2001a. Explanatory notes. *In* Moore, G.F., Taira, A., Klaus, A., et al., *Proc. ODP, Init. Repts.,* 190, 1–51 [CD-ROM]. Available from: Ocean Drilling Program, Texas A&M University, College Station TX 77845-9547, USA.

Shipboard Scientific Party, 2001b. Leg 190 summary. *In* Moore, G.F., Taira, A., Klaus, A., et al., *Proc. ODP, Init. Repts.,* 190: College Station TX (Ocean Drilling Program), 1–87.

Shipboard Scientific Party, 2001c. Site 1173. *In* Moore, G.F., Taira, A., Klaus, A., et al., *Proc. ODP, Init. Repts.,* 190, 1–147 [CD-ROM]. Available from: Ocean Drilling Program, Texas A&M University, College Station TX 77845-9547, USA.

Shipboard Scientific Party, 2001d. Site 1174. *In* Moore, G., Taira, A., Klaus, A., et al., *Proc. ODP, Init. Repts.,* 190, 1–149 [CD-ROM]. Available from: Ocean Drilling Program, Texas A&M University, College Station TX 77845-9547, USA.

Shipboard Scientific Party, 2002a. Explanatory notes. *In* Mikada, H., Becker, K., Moore, J.C., Klaus, A., et al., *Proc. ODP, Init. Repts.,* 196, 1–53 [CD-ROM]. Available from: Ocean Drilling Program, Texas A&M University, College Station TX 77845-9547, USA.

Shipboard Scientific Party, 2002b. Leg 196 summary: deformation and fluid flow processes in the Nankai Trough accretionary prism: logging while drilling and advanced CORKs. *In* Mikada, H., Becker, K., Moore, J.C., Klaus, A., et al., *Proc. ODP, Init. Repts.,* 196: College Station TX (Ocean Drilling Program), 1–29.

Wyllie, M.R.J., Gregory, A.R., and Gardner, G.H.F., 1958. An experimental investigation of factors affecting elastic wave velocities in porous media. *Geophysics,* 23:400.

Figure F1. Map showing the location of ODP Sites 1173, 1174, and 808 for Legs 190 and 196. The red box outlines the location of the three-dimensional seismic survey (Bangs et al., 1999; Moore et al., 1999). Depth contours are in kilometers. (Shipboard Scientific Party, 2002b).

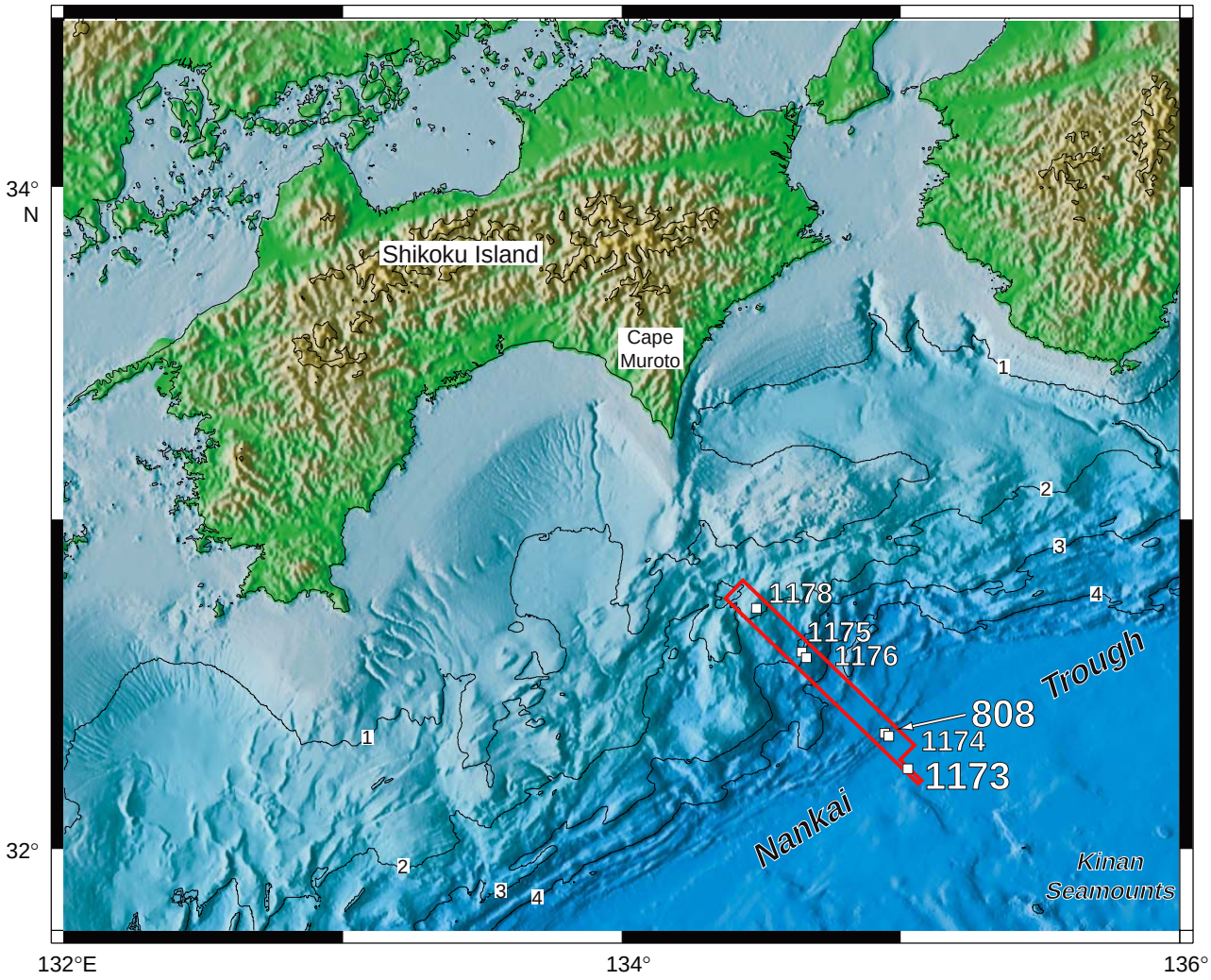

Figure F2. Cross section showing major structural features based on seismic reflection data from Hills et al. (2001). Site 1173, where there is little or no tectonic deformation in the sediments, is used as the reference site (Shipboard Scientific Party, 2002b). VE = vertical exaggeration.

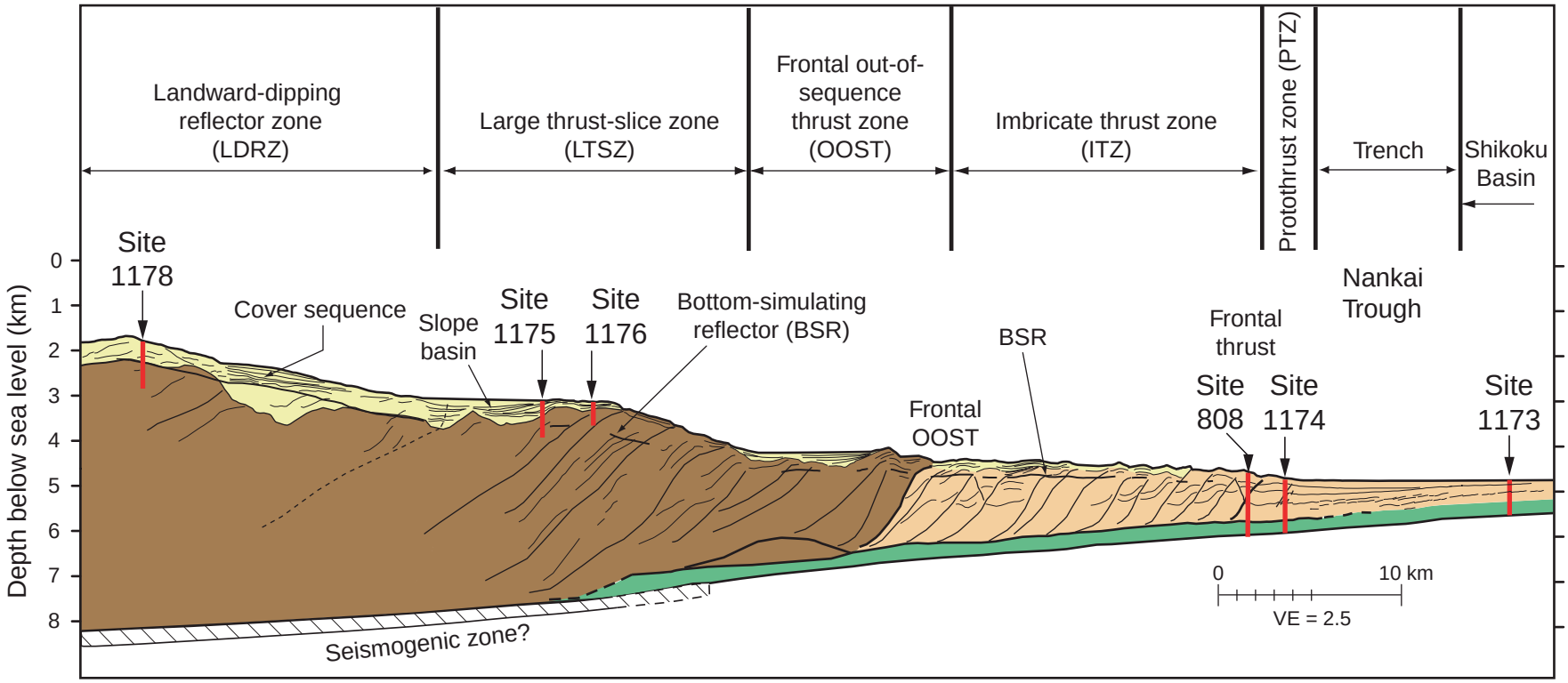

Figure F3. Stratigraphic column for Site 1173. Sites 1174 and 808 contain additional trench-fill sediments (Shipboard Scientific Party, 2001c).

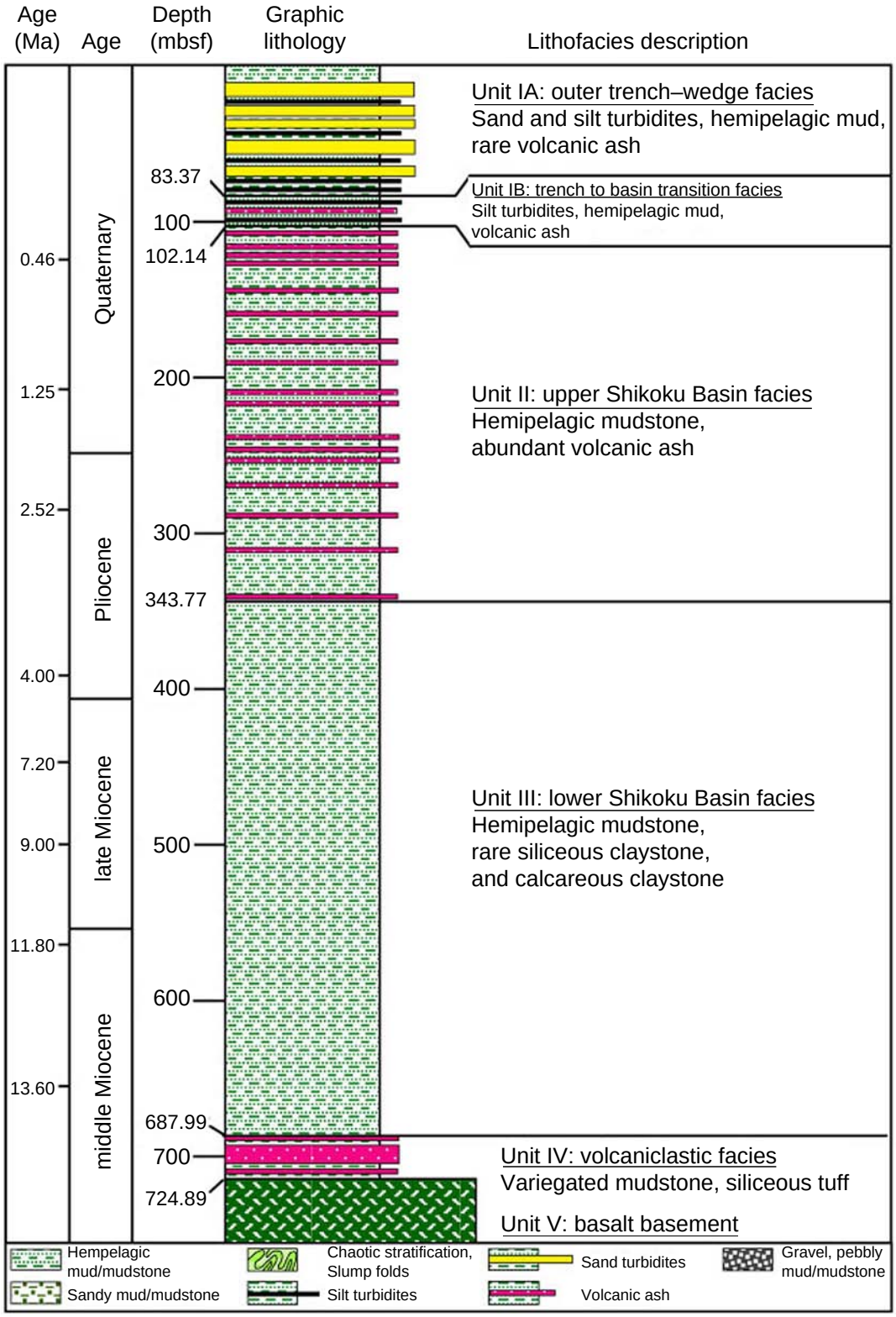

Figure F4. Core-based laboratory measurements of compressional velocity and porosity for Sites 1173, 1174, and 808. The proto-décollement for Site 1173 and the décollement for Sites 1174 and 808 are indicated by the black line. Velocity measurements are in the z-direction only. In situ corrections have not yet been applied to these data.

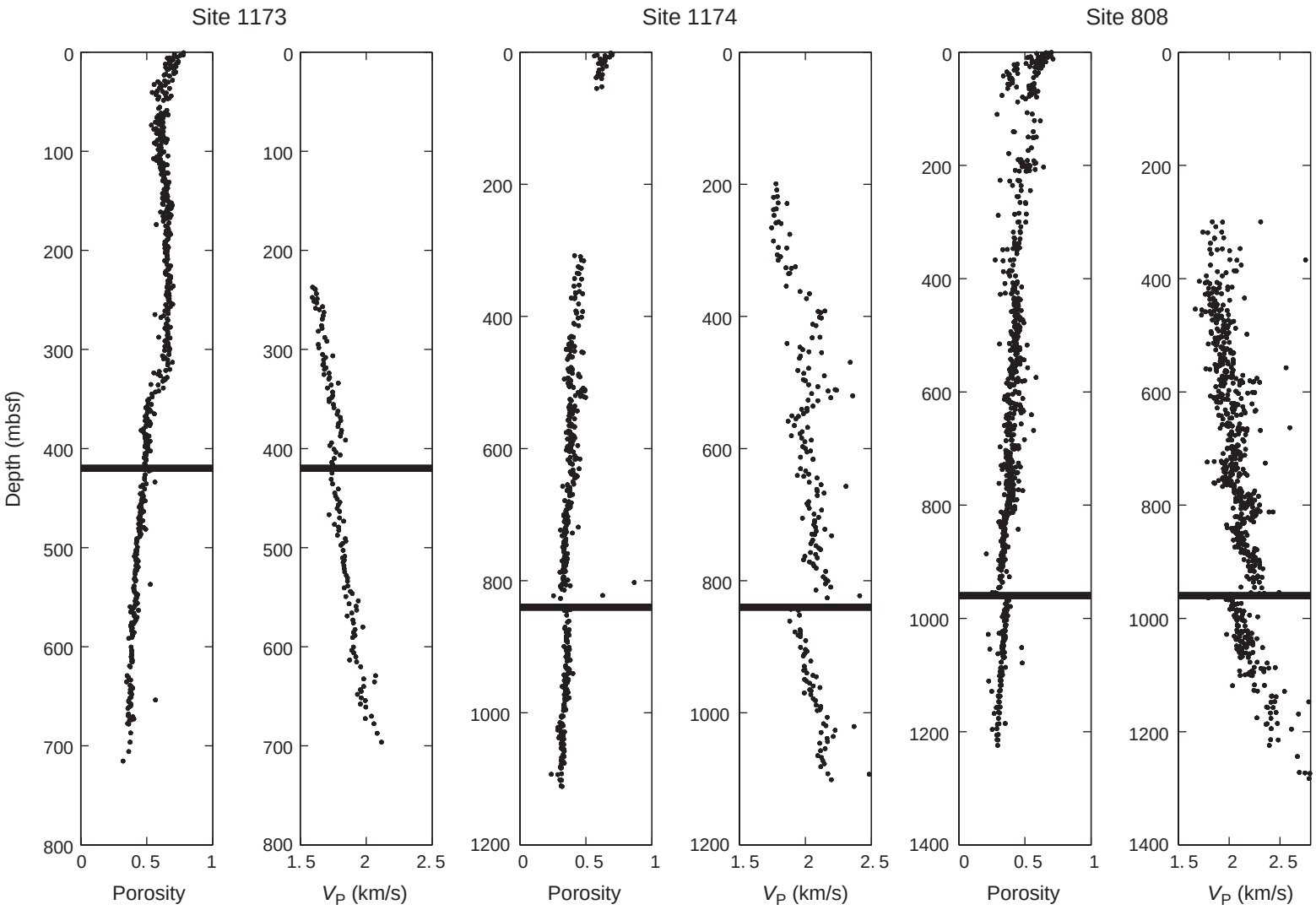

Figure F5. Core and wireline log porosity measurements for Site 1173. **A.** All available porosity data. **B.** Porosity data with corresponding depths to within 10 cm. (Note the change in depth scale between A and B).

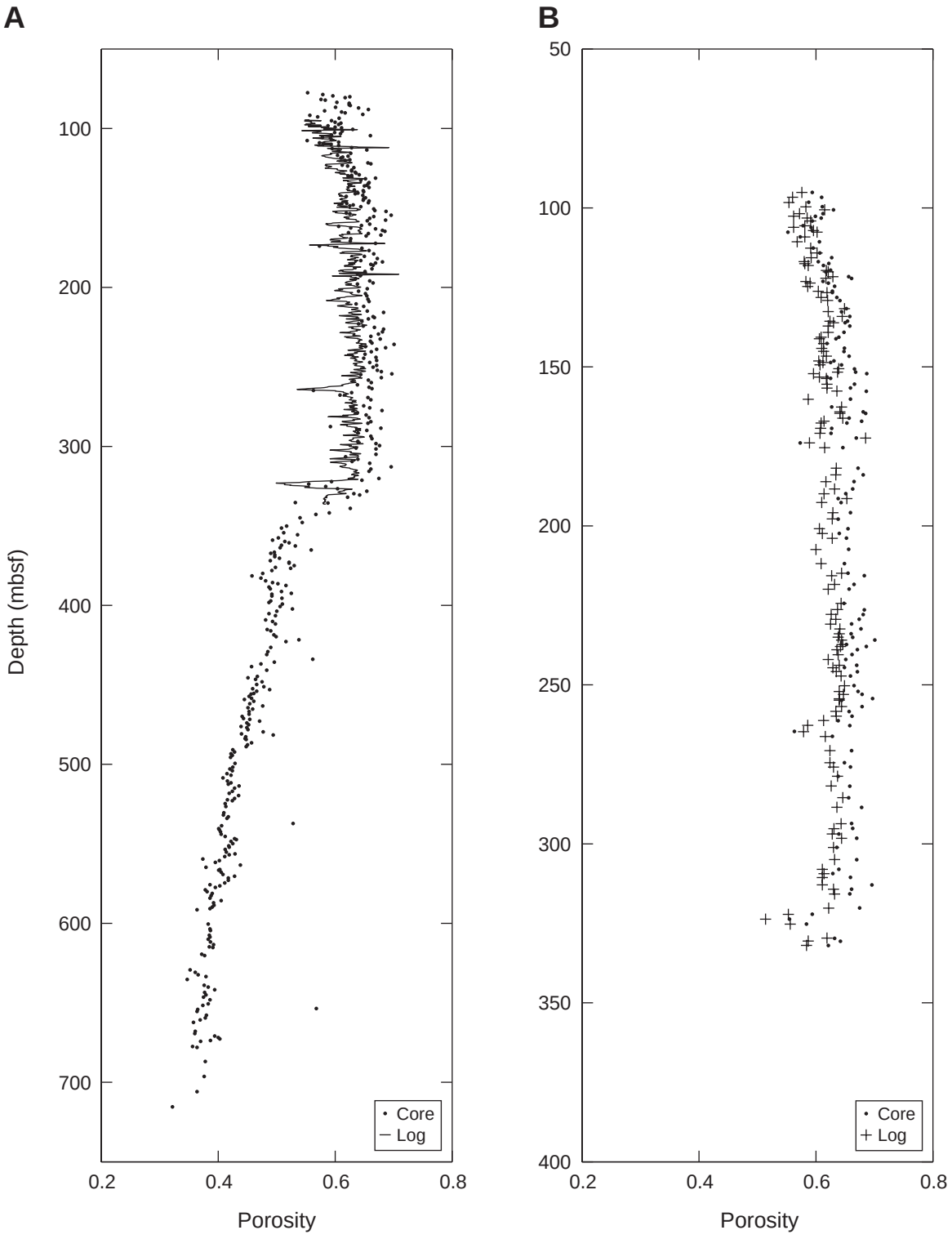

Figure F6. Core and LWD porosity measurements for Site 1173. **A.** All available porosity data. **B.** Porosity data with corresponding depths to within 10 cm.

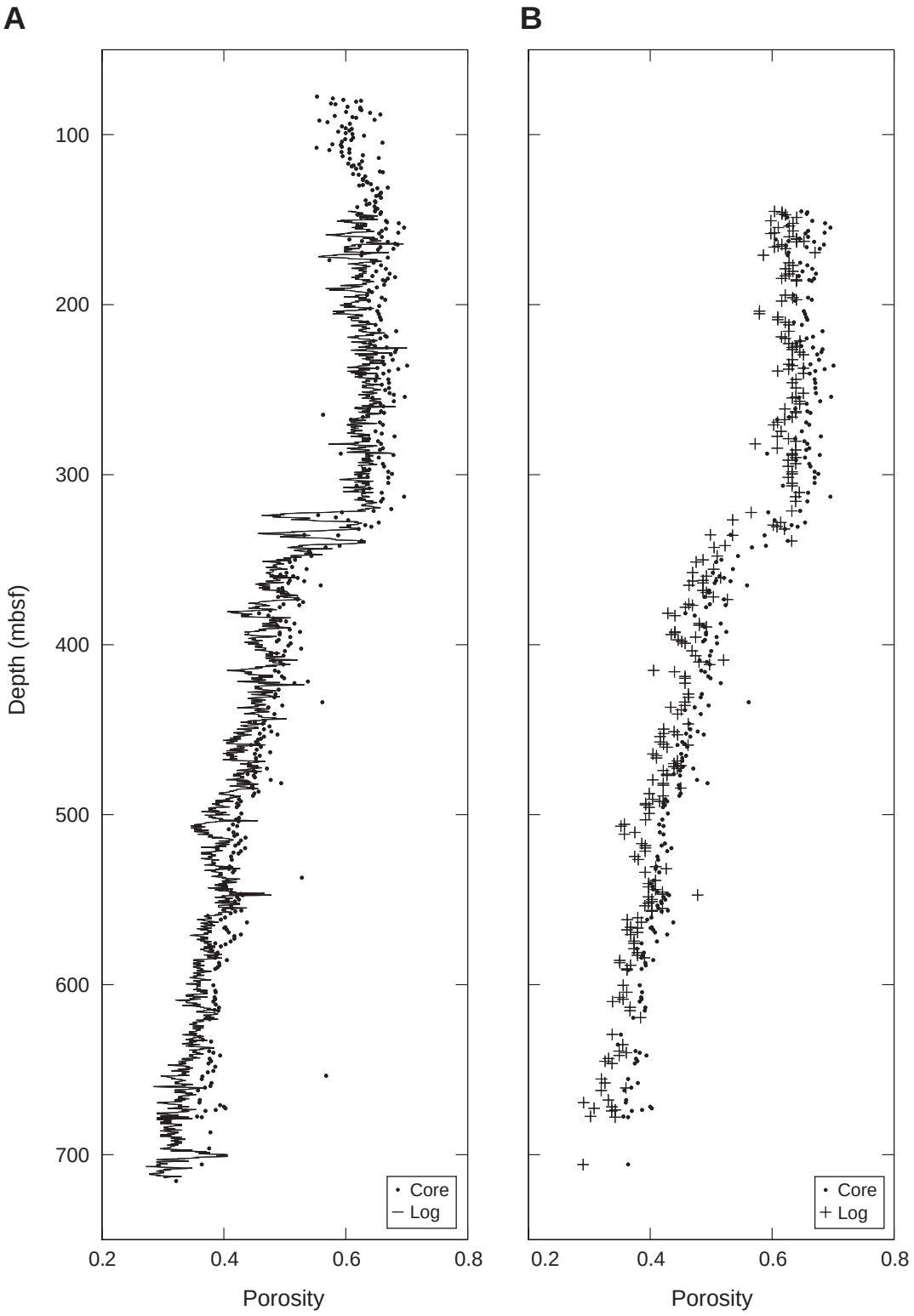

Figure F7. Core and wireline velocity measurements for Site 1173. **A.** All available velocity data. **B.** Data with corresponding depths. **C.** Difference in velocity between core and wireline measurements. (Note the change in depth scale between A and B).

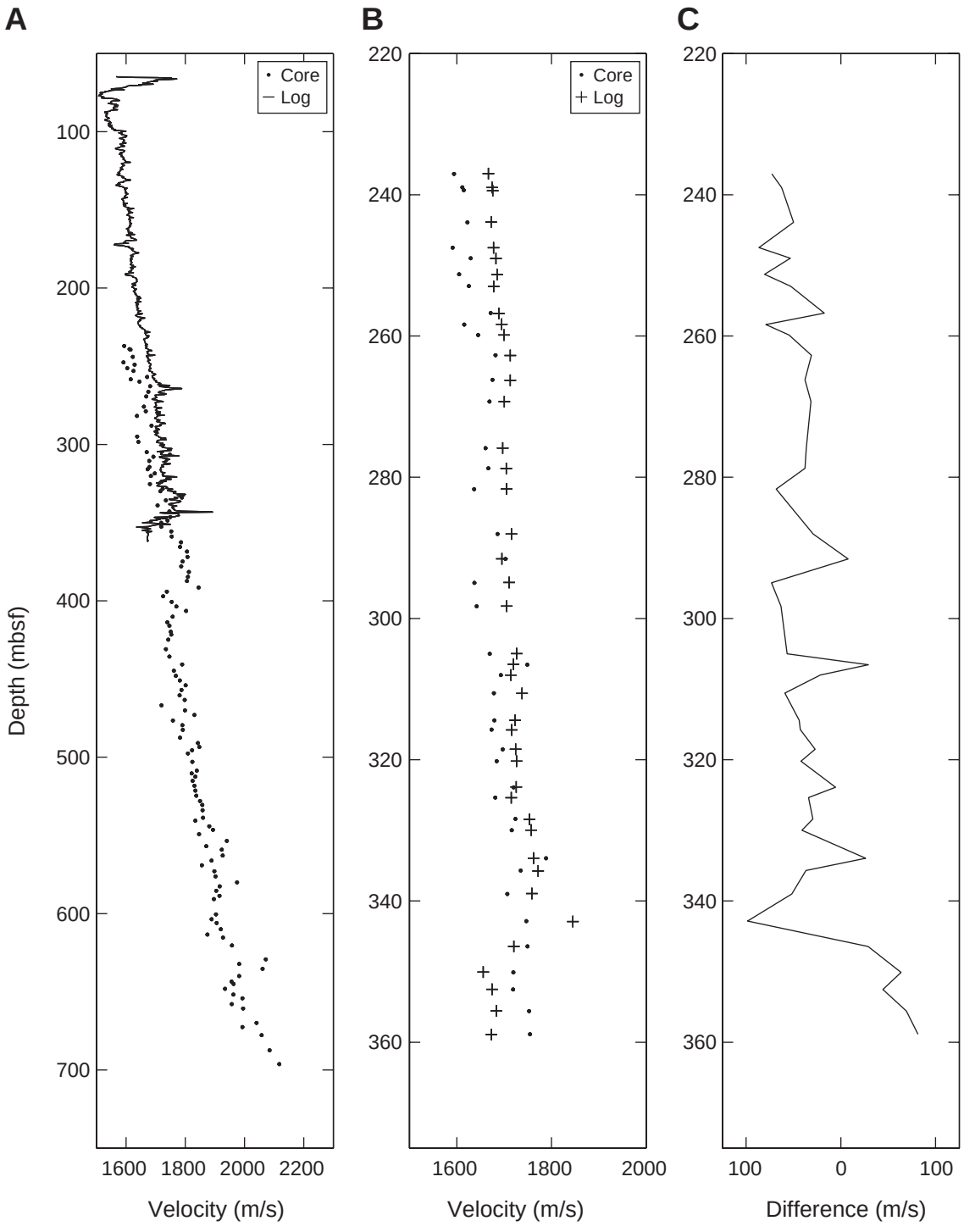

Figure F8. Compressional velocity as a function of porosity and shale fraction for (**A**) normal and (**B**) high consolidation (Erickson and Jarrard, 1998). Velocity is plotted for shale fractions of 0, 0.2, 0.4, 0.6, 0.8, and 1.

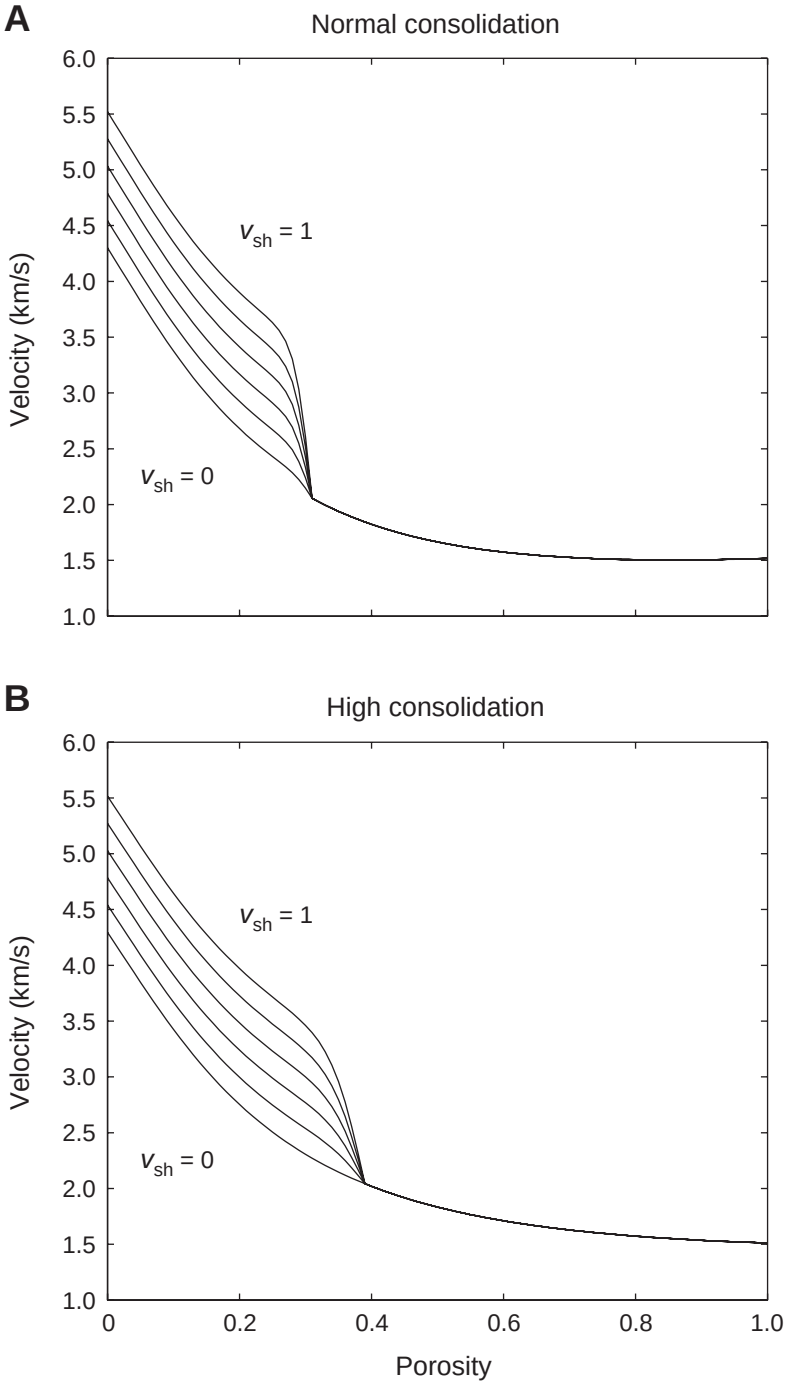

Figure F9. Calculated shale fraction log for Site 1173. The average shale fraction calculated is 0.32. The sand and shale baselines were taken from the logging-while-drilling (LWD) gamma ray log from Site 808.

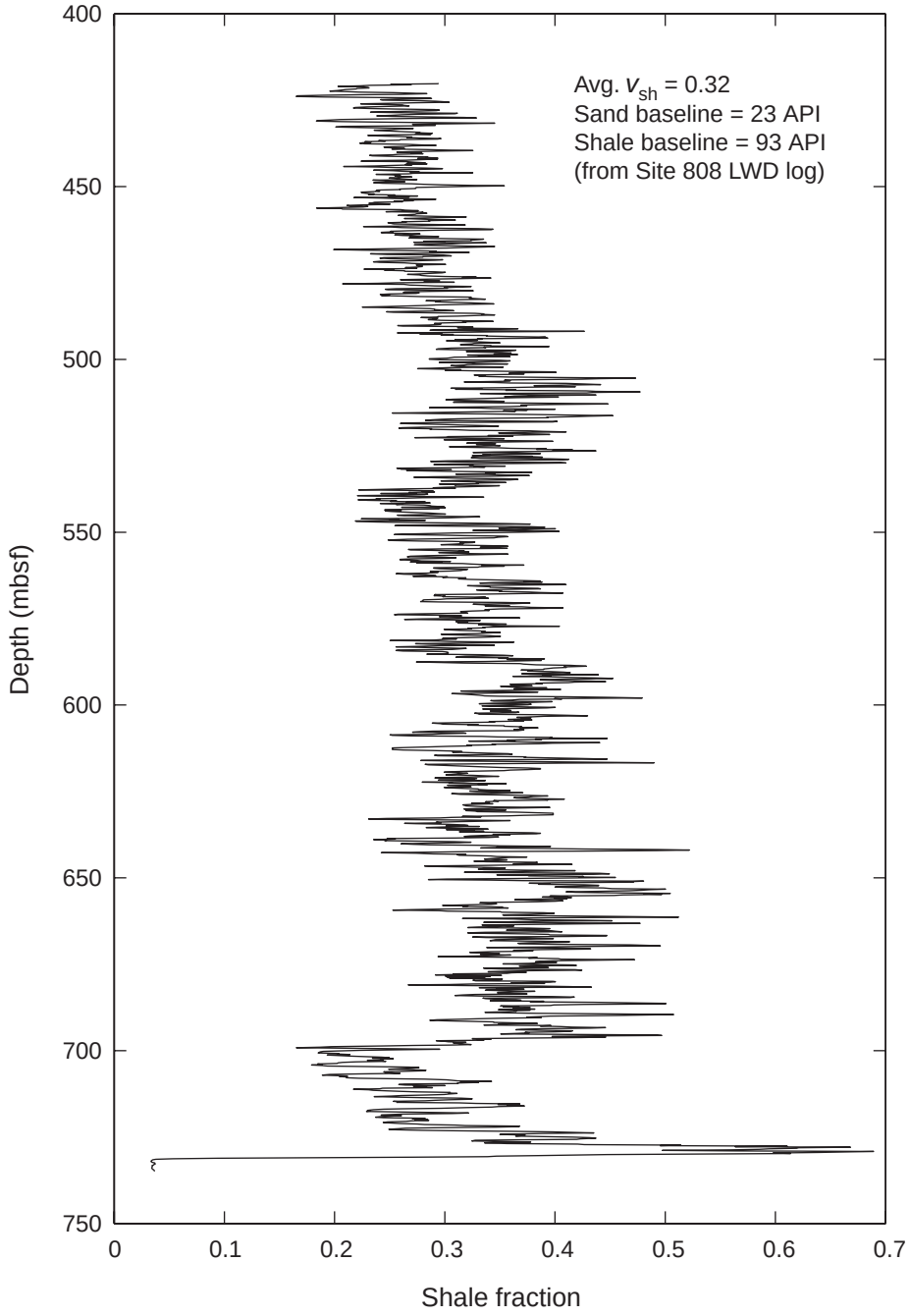

Figure F10. Velocity vs. porosity for in situ corrected core data for Sites 1173, 1174, and 808. **A.** Sediments above and below the décollement (projected décollement at Site 1173). **B.** Underthrust sediments.

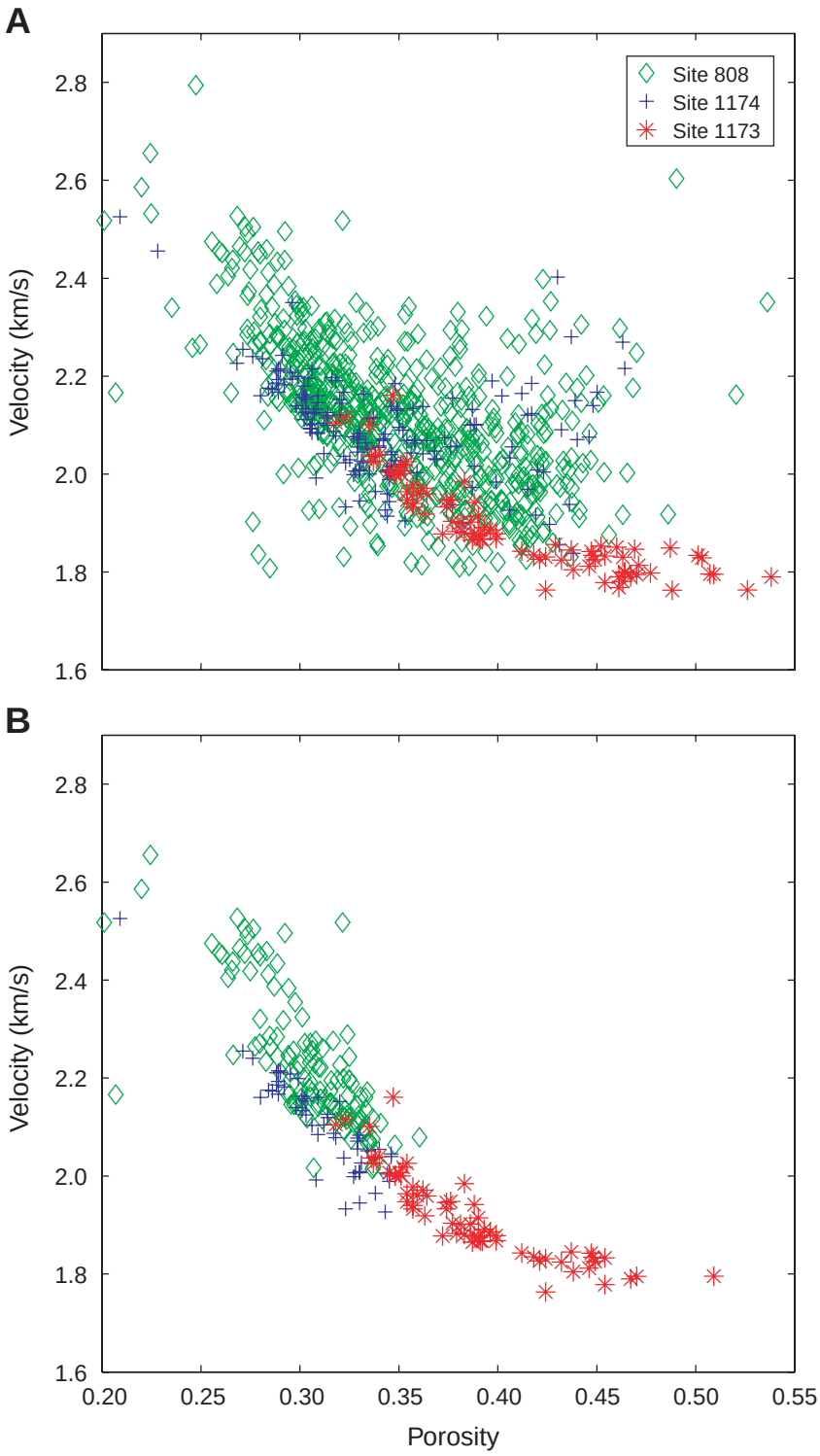

Figure F11. Empirical velocity-porosity formulations for the underthrust sediments for Sites 1173, 1174, and 808. The least-squares fit (solid black line) is plotted for a shale fraction of 1. The formulations for normal and high consolidation (Erickson and Jarrard [E&J], 1998) are plotted for shale fractions of 1 as well as the formulation from Hyndman et al. (1993).

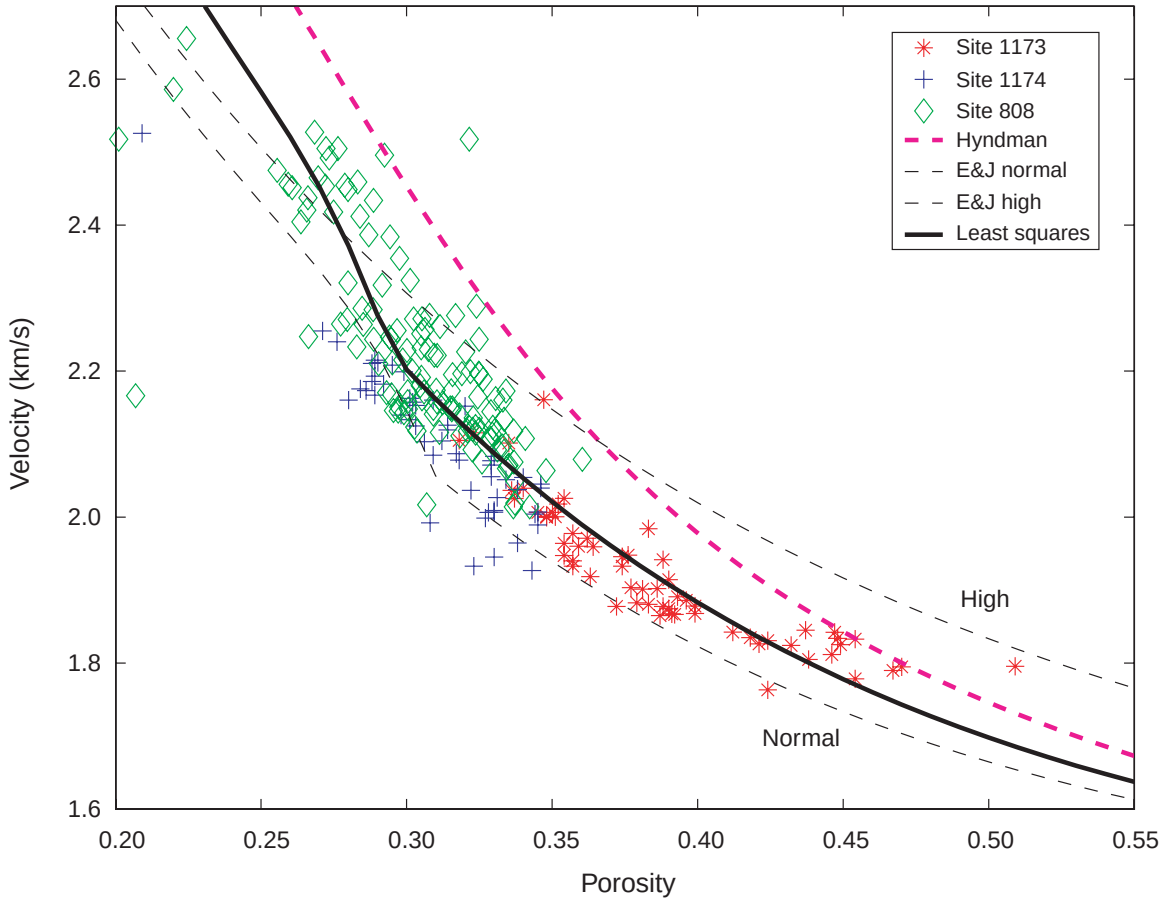

Table T1. Results of the parameter fitting for the best-fit formulation.

				Erickson and Jarrard (1998)	
Parameter	Fit	Error (±)	Error (%)	Normal 0.739	High 1.11
A	0.746	0.379	51		
B	0.532	0.327	61	0.552	0.178
C	0.124	0.171	137	0.13	0.135
v_{sh}	1.057	0.041	4	—	—
ϕ_c	0.295	0.006	2	0.31	0.39

Note: The Erickson and Jarrard (1998) parameters for normal and high consolidation are listed for comparison.